Influence of elevated temperatures on CFRP strengthening systems

Maria da Graça Roquette Instituto Superior Técnico

Abstract

This paper presents experimental and numerical investigations about the influence of elevated temperatures on carbon fibre reinforced polymer (CFRP) strengthening systems. The experimental campaign comprised shear and tensile tests performed at elevated temperatures (up to 120 ºC) on epoxy adhesive typically used as a bonding agent in CFRP systems. In both test series, the mechanical response of the adhesive as a function of temperature was assessed, namely in terms of load *vs.* displacement curves, stress *vs.* strain/distortion curves, stiffness, strength and failure modes. The results obtained confirmed that both shear and tensile properties present a considerable reduction with increasing temperatures: at 70 ºC the shear and tensile strengths are both reduced to around 15% compared to ambient temperature figures, while the tensile and shear moduli can be considered negligible at that temperature. In the numerical investigation, three-dimensional (3D) finite element (FE) models were developed to simulate double-lap shear test performed on concrete blocks strengthened with CFRP strips installed according to either the externally bonded reinforcement (EBR) and near surface mounted (NSM) techniques. Two distinct modelling strategies for the concrete-CFRP bond were adopted: (i) to explicitly simulate the bonding adhesive considering the mechanical properties of the adhesive determined in the experimental campaign and assuming a perfect bond between all constituent materials; and, alternatively, (ii) to simulate the CFRP-concrete interaction by means of global bilinear bond *vs* slip laws for different temperatures that are available in the literature. Comparisons between numerical and previous experimental results confirmed that the strategy adopted in (i) provides generally stiffer estimates of the concrete-CFRP bond (*e.g.*, 90 °C, 3.1 to 5.2 times); as expected, the numerical results obtained with the strategy (ii) showed a remarkable agreement with the experimental results. This numerical study (i) confirmed that in order to accurately simulate the behaviour of CFRP-concrete bond at elevated temperatures it is necessary to consider slip at the interfaces of the materials and (ii) allowed quantifying the relative contribution of interfacial slip and adhesive distortion to the concrete-CFRP bond at elevated temperature.

Keywords: Epoxy adhesive, CFRP strengthening of RC structures, externally bonded reinforcement (EBR) technique, near surface mounted (NSM) technique, bond behaviour, elevated temperatures.

1. Introduction

Over the past 25 years, carbon fibre reinforced polymer (CFRP) materials have been finding increasing applications in rehabilitation and strengthening of reinforced concrete (RC) structures. This increasing interest on CFRP materials stems from their indisputable advantages over traditional materials (in particular steel), such as high strength-to-weight ratio, corrosion resistance and ease of application [1].

In spite of the above-mentioned advantages over traditional strengthening materials/techniques, in applications where structural fire ratings are required (*e.g.* buildings), the attempts to apply these strengthening systems have been hampered due to unknowns about the reduction of their mechanical and bond properties at elevated temperatures. In fact, when the glass transition temperature (T_g) of the most susceptible material to this type of action (generally the epoxy-based adhesives, which present lower T_g than that exhibited by CFRPs) is reached, its mechanical properties are severely deteriorated and, consequently, the structural effectiveness of the strengthening system is substantially affected [2].

Even though the fire performance exhibited by CFRP systems is known to be poor and the bonding adhesive has been identified as the most susceptible constituent to the mechanical degradation of the system when exposed to elevated temperatures, the (limited) research available is mainly focused on the bond degradation rather than on the characterization of the mechanical properties of the adhesives themselves; further studies are clearly needed to fill this gap in current knowledge.

2. Literature review

The influence of temperature on the mechanical properties of bonding adhesives used in CFRP strengthening systems has been addressed in a very limited number of studies. Bascom and Cottington [3] reported a tensile strength reduction on an epoxy-based adhesive with a T_g of 68ºC (test method not specified) of 35% at 50 ºC (maximum temperature tested). Moussa *et al.* [4] reported that at 60 ºC the strength and stiffness of an epoxy adhesive (T_g = 48 ºC, determined through DSC) were almost negligible.

Besides the aforementioned experimental studies, most prior investigations have focused on the bond behaviour between concrete and CFRP strips. In general, the existing studies concerning the influence of temperature on these bonded joints showed remarkable bond strength reductions for temperatures above the adhesives' T_g. However, there are some contradictory results regarding the bond strength variation for temperatures below T_g - in fact, some studies reported bond strength increases (when compared to those at ambient temperature) [5–8], whereas in others bond strength reductions were obtained [9–13]. For instance, Wu *et al.*[9] and Gamage *et al.*[10] reported a consistent decreasing failure load with increasing temperature. In opposition, Blontrock[5]

and Klamer *et al.* [6] conducted double-lap shear tests and reported increasing failure loads for temperatures lower than the T_g of the adhesive. However, it is noteworthy that in the latter studies, in which the bond strength increased at elevated temperatures below T_g, the specimens were all conditioned at elevated temperature for long durations prior to structural testing. It is thus likely that the occurrence of post-curing of the resin improved the bond performance.

Regarding the numerical studies on this topic, a few finite element (FE) models were developed to simulate the influence of temperature on the bond behaviour of CFRP-concrete bonded joints. In order to accurately predict the structural response of these bonded connections, such numerical analyses include bond *vs.* slip relations for the CFRP-concrete interfaces at elevated temperatures. The most common approach is to simulate the bond behaviour by means of bilinear [14] or non-linear bond *vs.* slip relationships [15].

Klamer [7] simulated double-lap shear tests performed at elevated temperature on concrete blocks strengthened with externally bonded (EBR) CFRP strips. Two-dimensional (2D) FE models were developed using the commercial software DIANA, in which the bond between the CFRP strips and the concrete was simulated with bilinear bond *vs.* slip relationships. For temperatures up to the adhesive's T_g (62 °C; test method not specified), a typical bond *vs.* slip relation for ambient temperature was modified to take into account the effect of the reduced Young's modulus of the adhesive. However, for temperatures above the adhesive's T_g, this procedure did not provide good results.

Arruda *et al.* [16] simulated double-lap shear tests, in which the influence of the strengthening technique, either EBR or near surface mounted (NSM), on the bond behaviour with temperature was evaluated. Three-dimensional (3D) FE models were developed, using the commercial package ABAQUS, in which the global bond behaviour of the strengthening systems was simulated by means of bilinear bond *vs.* slip laws; these were derived based on an inverse analysis, in order to maximize the agreement between experimental and numerical results in terms of (i) failure loads, (ii) load *vs.* slip responses, and (iii) strain distributions along the bonded length. Besides the good agreement between numerical and experimental results, it was also possible to accurately simulate the failure modes experimentally observed.

The brief literature review presented above showed that: (i) very few experimental studies are available concerning the tensile properties of the bonding adhesives as function of temperature and none concern their shear properties in spite of their relevance; and (ii) the investigation efforts made so far to describe the bond behaviour between CFRP and concrete are very limited, and in some cases are contradictory. These shortcomings were the main motivation of the present study, which aims at providing contributions to the two above-mentioned topics.

This paper presents experimental and numerical investigations about the influence of elevated temperatures on CFRP strengthening systems. In the experimental campaign the mechanical response in tension and shear of an epoxy adhesive (typically used as a bonding agent in CFRP strengthening systems) was assessed, as a function of temperature. In the numerical investigation, 3D FE models were developed to simulate double-lap shear test performed on concrete blocks strengthened with CFRP strips for the two strengthening techniques (EBR or NSM). Two distinct modelling strategies for the concrete-CFRP bond were adopted: (i) to explicitly simulate the bonding adhesive considering its mechanical as a function of temperature as determined in the experimental campaign and assuming a perfect bond between all constituent materials; and, alternatively, (ii) to simulate the CFRP-concrete interaction by means of global bilinear bond *vs* slip laws for different temperatures that are available in the literature

3. Experimental investigation

3.1. Adhesive's description

The adhesive analysed in the present experimental campaign was a conventional two-component epoxy adhesive typically used to bond CFRP strips to concrete, with the commercial designation *S&P Resin 220* and a glass transition temperature of 47 °C, determined from dynamic mechanical analyses (DMA, dual cantilever setup, heating rate of 1 °C/min), defined based on the onset of the storage modulus curve decay.

3.2. Shear tests at elevated temperatures

3.2.1. Specimens geometry and preparation

The specimens were prepared according to ASTM 5379/D 5379M – 05 [17] specifications. The coupons' geometry (*cf.* **Fig. 1**) consisted of rectangular strips (75×20 mm, 8 mm thick) with two symmetrical centrally located V-notches. These adhesive coupons were left at 20 °C for about 7 months in order to guarantee a high-degree of ambient-temperature cure.

The preparation of test specimens can be summarized in two stages: (i) the execution of a deep hole along the longitudinal direction of the specimen (17.5 mm of depth; 0.25 mm of diameter), where a thermocouple wire (type K) was introduced to measure the temperature inside the specimen during the heating phase; and (ii) the marking of eight reading points/targets (*cf.* **Fig. 1**) used for the videoextensometry technique adopted for measuring the deformations of the test specimens (*cf.* next section).

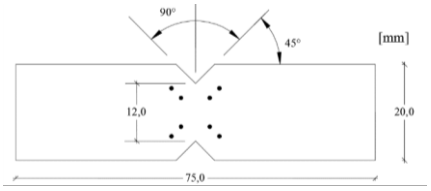

Fig. 1 – Shear coupons: dimensions and target scheme.

3.2.2. Test setup, instrumentation and procedure

The shear tests were performed according to the V-Notched Beam Test [17], in which the specimens are loaded in a mechanical testing machine by a special fixture (*cf.* **Fig. 2** a)). The specimens were first heated up to temperatures of 20 ºC, 35 ºC, 50 ºC, 70 ºC, 90 ºC and 120 ºC and then load up to failure (maintaining a constant temperature in the specimens). For each temperature, at least three valid tests were carried out.

The tests were performed in a thermal chamber (*Tinius Olsen* with inner dimensions 605×250×250 mm) attached to a universal testing machine (*Instron*; 250 kN capacity). Two type K thermocouples (0.25 mm conductor diameter) were used to measure the test specimens' temperature (installed inside the drilled hole) and the air in the thermal chamber. During the heating stage the average rate of heating was 14 ºC/min (measured in the air inside the thermal chamber); once the predefined target temperature was attained and the coupons' temperature stabilized, the specimens were loaded up to failure under displacement control (speed of 0.5 mm/min); note that the coupons' temperature was kept constant during the loading stage.

During the loading stage, the cross-head displacement of the test machine and the applied load were recorded, as well as the displacements of the eight points/targets (previously marked on the test specimens, *cf.* **Fig. 1**) through the videoextensometry technique (*cf.* **Fig. 2** b)). The equipment used for the latter technique was the following: a high definition *Sony* video camera (model *XCG-5005E*, *Fujinon – Fujifilm HF50SA-1* lens), and a computer software (*LabView*). The shear modulus was estimated by the slope (obtained by linear regression) of the stress *vs.* distortion curves between 20% and 50% of the maximum shear stress.

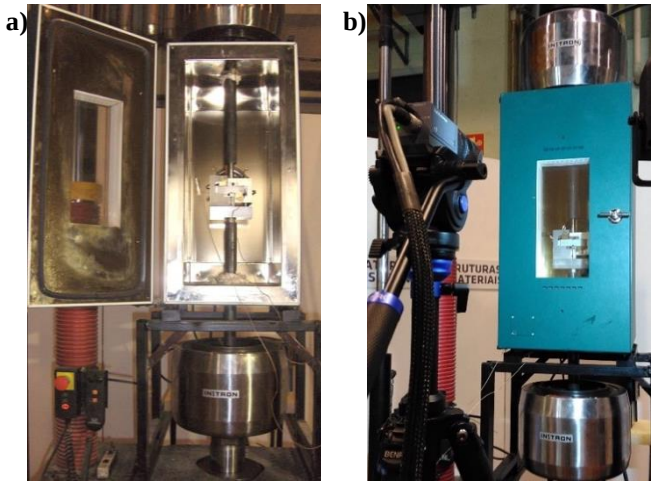

Fig. 2 – Shear tests setup: a) test fixture positioned inside of the thermal chamber; b) positioning of the video extensometer according to the viewing window of the thermal chamber.

3.3. Tensile tests at elevated temperatures

3.3.1. Specimens geometry and preparation

The dob-bone shaped samples (*cf.* **Fig. 3**), prepared according to ISO 527-1 [18] specifications, had outer dimensions of 170 × 20 mm and were 4 mm thick. These adhesive coupons were left at 20 °C for about 7 months in order to guarantee a high degree of ambient temperature cure. Four targets were marked on the front face of the specimens, as illustrated in **Fig. 3**, which is related to the adopted technique for measuring the deformations of the test pieces (*cf.* next section).

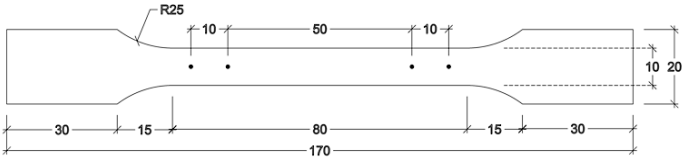

Fig. 3 – Tensile coupons: dimensions and target scheme.

3.3.2. Test setup, instrumentation and procedure

Tensile tests, performed according to ISO 527-1 [18], were conducted by fixing both ends of the specimens between two grips, as shown in **Fig. 4**. For each temperature, at least three valid tests were carried out.

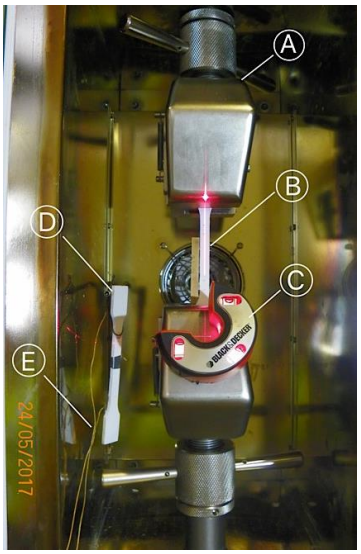

Fig. 4 – Positioning of the test specimens inside of the thermal chamber: A) tensile test grips; B) test specimen; C) leveller; D) temperature measurement sample; E) type K thermocouple wires.

The procedure was similar to that adopted for the shear tests: the specimens were first heated up inside of a thermal chamber at an average heating rate of 16 ºC/min (temperature of the air in the thermal chamber) up to temperatures of 20 ºC, 35 ºC, 50 ºC, 70 ºC, 90 ºC or 120 ºC; subsequently, at constant temperature, a tensile load was applied under displacement control (speed of 0.5 mm/min) up to failure. The applied load, the cross-head displacement of the test machine and the displacements of the four points/targets (previously marked on the test specimens, *cf.* **Fig. 3**) were recorded. The tensile modulus was estimated by the slope (obtained by linear regression) of the stress *vs.* strain curves between 20% and 50% of the maximum tensile stress.

3.4. Experimental results and discussion

3.4.1. Shear tests at elevated temperatures

Fig. 5 presents the load *vs.* displacement curves (total displacement of the testing machine) for one representative specimen of each target temperature. This figure shows the global stiffness and maximum load reductions with temperature (especially from 35 ºC to 50 ºC). Moreover, for temperatures below T_g (*i.e.* 20 °C and 35 °C), an approximately linear behaviour up to failure is observed (brittle behaviour). However, for higher temperatures the curves present non-linear behaviour, especially at 50 °C and 70 °C, which is due to the mechanical changes associated with the glass transition process of the adhesive.

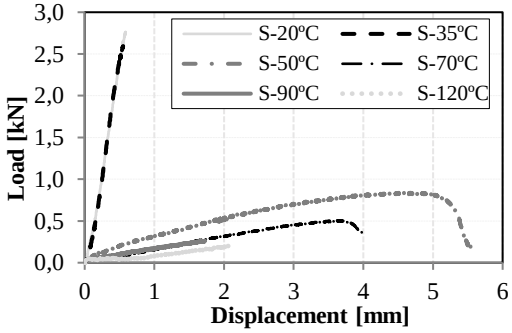

Fig. 5 – Load *vs.* displacement curves in shear tests for representative specimens of all tested temperatures.

Fig. 6 shows the shear stress *vs.* distortion curves for one representative specimen of each tested temperature; as can be observed, both the shear stiffness and strength present significant degradation with the temperature increase (*cf.*, **Tab. 1**). Furthermore, in general, an approximate linear behaviour is observed up to failure (brittle behaviour), except at 50 ºC and 70 ºC; for these temperatures, after the maximum shear stress is reached, there is a progressive reduction of the shear stress together with an increase in the adhesive distortion. Finally, it can also be seen that the maximum distortion presents a non-monotonic variation with temperature (*e.g.*, the distortion capacity increases from 35 ºC to 50 ºC, but decreases from 50 ºC to 90 ºC), unlike the variation of the maximum shear stress, which decreases monotonically with increasing temperature.

The typical failure modes observed in all experimental series are shown in **Fig. 7**. In general, three types of failure were observed: (i) two inclined and parallel cracks, both beginning at the vertices of the test pieces notches (mode obtained at 20 °C and 35 °C); (ii) according to a single plane, in the central zone of the specimens (smallest cross-sectional area; mode obtained at 50 °C and 70 °C); and finally (iii) two curved cracking surfaces (mode obtained at 90 °C and 120 °C).

It should be noted how the failure mode is related to the behaviour of the shear stress *vs.* distortion curves: (i) test specimens whose rupture occurred with the formation of two slits (20 °C, 35 °C and 90 °C, 120 °C) correspond to more linear curves; (ii) tests with distinct fractures (at 50 °C and 70 °C), where the rupture occurred through the central section of the specimen, correspond to non-linear curves.

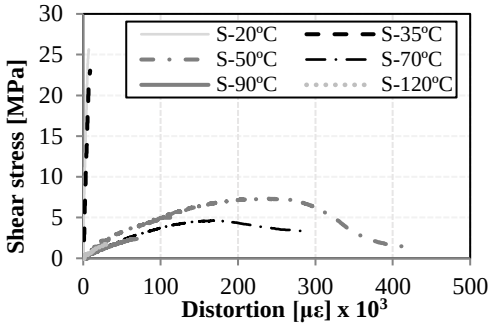

Fig. 6 – Shear stress *vs.* distortion curves for representative specimens of all tested temperatures.

Tab. 1 – Shear strength and shear modulus for the considered temperatures (average ± standard deviation).

T [°C]	$\tau_{u,avg}$ [MPa]	$G_{,avg}$ [MPa]
20	25.1 ± 1.5	4611.1 ± 565.9
35	21.8 ± 1.8	2950.6 ± 685.8
50	8.1 ± 1.3	50.5 ± 9.1
70	4.1 ± 0.5	36.2 ± 2.6
90	2.3 ± 0.3	37.8 ± 5.4
120	2.0 ± 0.3	34.5 ± 16.1

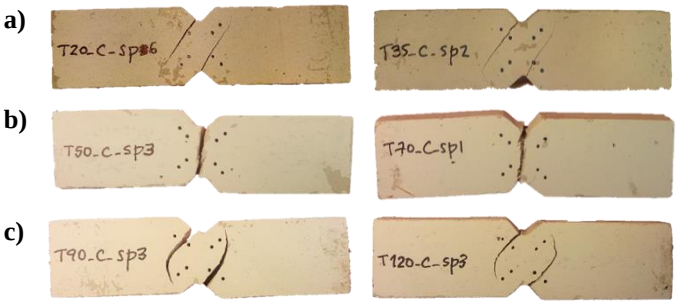

Fig. 7 – Typical failure modes of specimens tested at: a) 20 °C and 35 °C; b) 50 °C and 70 °C; and c) 90 °C, 120 °C.

3.4.2. Tensile tests at elevated temperatures

Fig. 8 presents the load *vs.* displacement curves (total displacement of the testing machine) for one representative specimen of each tested temperature. It can be seen that, besides the overall stiffness reduction, the tensile strength also shows a significant degradation with the increasing temperature.

Fig. 9 shows the tensile stress *vs.* strain curves, also for one representative specimen of each tested temperature. Similar conclusions can be drawn to those made for the shear tests (*cf.* section 3.4.1); for instance, in addition to a remarkable shear stiffness reduction, the tensile strength also presents a significant degradation with temperature (*cf.* **Tab. 2**). Moreover, a change in the curves behaviour is observed as temperature increases, especially from 35 ºC to 50 ºC. Finally, it can also be seen that the maximum strain presents a non-monotonic variation with temperature, unlike the variation of the maximum tensile stress, which decreases monotonically with increasing temperature

The typical failure mode observed in all tensile test series (tensile rupture at the central length of the dob-bone shaped specimens) is shown in **Fig. 10**.

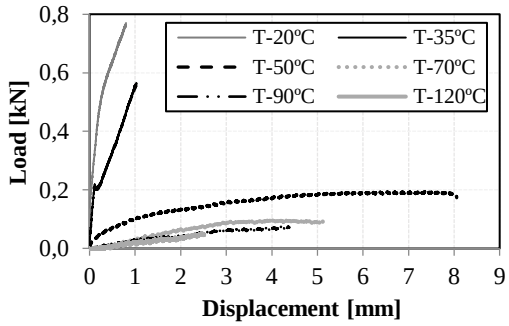

Fig. 8 – Load *vs.* displacement curves in tensile tests for representative specimens of all tested temperatures.

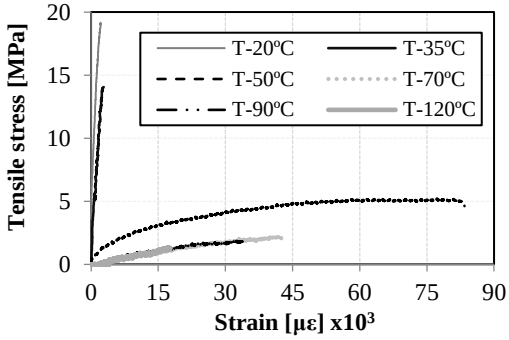

Fig. 9 – Tensile stress *vs.* strain curves for representative specimens of all tested temperatures.

Tab. 2 – Tensile strength and elastic modulus for the considered temperatures (average ± standard deviation).

T [°C]	$\sigma_{u,avg}$ [MPa]	E_{avg} [MPa]
20	16.6 ± 1.9	8205.3 ± 290.1
35	12.2 ± 1.1	6675.3 ± 801.3
50	5.2 ± 0.1	183.2 ± 24.1
70	2.4 ± 0.2	82.9 ± 21.8
90	1.8 ± 0.2	87.3 ± 30.5
120	1.6 ± 0.3	65.0 ± 47.1

Fig. 10 – Typical failure mode of a tensile test specimen.

3.4.3. Modelling of properties degradation with temperature

Several authors have proposed mathematical expressions based on semi-empirical models to simulate the evolution of various properties of FRP materials as a function of temperature. One of the most used models is the one proposed by Gibson *et al.* [19], in which the variation of a generic mechanical property P with temperature T, can be described by the following equation,

$$P(T) = P_u - \frac{P_u - P_r}{2} \times \left(1 + \tan h\left[k'\left(T - T_{g,mech}\right)\right]\right) \qquad (1)$$

where P_u is the property at ambient temperature and P_r is the property after glass transition (but before decomposition); k' and $T_{g,mech}$ are parameters obtained by fitting the experimental data. This section presents the calibration of equation (1) to the experimental data obtained in the present study for both shear and tensile properties.

Fig. 11 and **Fig. 12** illustrate the normalized strength and modulus degradation curves, respectively, as well as the experimental results of the shear and tensile tests. As can be observed, a good agreement between the prediction curves and the experimental results was obtained; these figures also confirm that the reduction of the stiffness properties with temperature is steeper than that exhibited by the corresponding strengths (as previously referred); in fact, both shear and tensile modulus can be considered negligible at temperatures above 70 °C. In both figures the normalized storage modulus curve, obtained from DMA tests on the same adhesive, is also shown (heating rate of 1 °C/min [20]); although the nature of the experimental tests performed in the present study is significantly different from that of the DMA tests, and therefore these should not be directly compared, both provide relevant information regarding the degradation of the material's stiffness as a function of temperature. For example, by comparing the curves shown in **Fig. 12**, it can be seen that, according to the Gibson *et al.* [19] model, the most pronounced modulus reductions occur as the temperature approaches 40 ºC, which is slightly lower than the adhesive's T_g (47 ºC, determined from the storage modulus curve). However, it is worth mentioning that for a more detailed analysis of these comparisons one should obtain more experimental results, especially between 35 °C and 50 °C (range of temperatures for which the highest reductions in mechanical properties were observed).

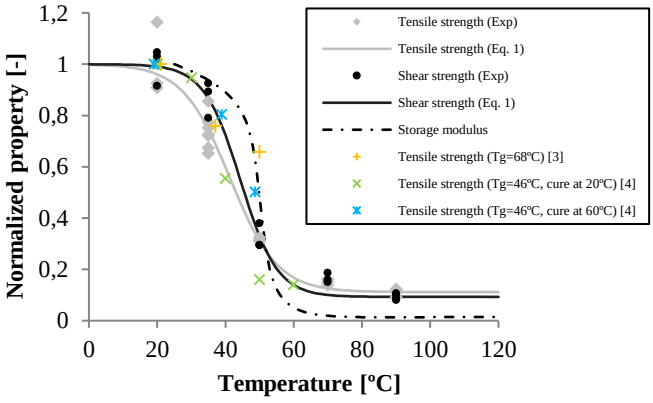

Fig. 11 – Prediction curves (and experimental results) of the tensile and shear strength of the adhesive as a function of temperature.

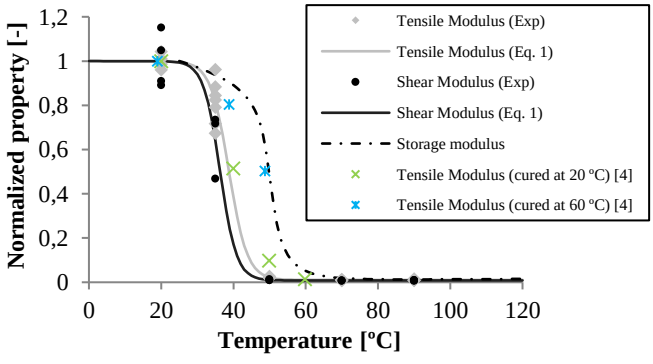

Fig. 12 – Prediction curves (and experimental results) of the tensile and shear modulus of the adhesive as a function of temperature.

4. Numerical investigation

4.1. Introduction and objectives

The structural response of the CFRP-concrete bonded joint stems from (i) the contribution of both interfaces (CFRP-adhesive and adhesive-concrete), whose actual behaviour can be defined by the corresponding non-linear bond *vs.* slip laws, together with (ii) the adhesive constitutive relationship (mainly its behaviour under pure shear). However, due to the complexity of the characterization of such interfaces and materials (especially at elevated temperatures), most of the studies available in the literature simulate the bond behaviour between concrete and CFRP by simplified/global laws, representatives of the overall response of the joint.

The study presented in this section comprised the numerical simulation of double-lap shear tests on RC blocks strengthened with CFRP strips, applied according to either EBR or NSM techniques, and performed at 20 °C, 55 °C and 90 °C (tests performed by Firmo *et al.* [11, 13]). The main objective of this numerical study is to simulate the mechanical response of CFRP-concrete joints at elevated temperatures through two different modelling strategies for the concrete-CFRP bond behaviour: (i) explicitly simulating the adhesive layer, using the material properties determined in this study and neglecting the bond laws at both interfaces; and (ii) simulating the CFRP-concrete interaction by bilinear global bond *vs.* slip laws available in the literature.

To achieve the aforementioned goals, two different 3D FE models were developed in ABAQUS [21]: (i) one model designated as "adhesive model", in which the temperature-dependent mechanical properties of the adhesive presented in section 3 (that were independently determined) were considered, as well as those of the other materials; and (ii) the model referred to as the "interface model", in which the CFRP-concrete bond was simulated through global bond *vs.* slip relations as a function of temperature calibrated by Arruda *et al.* [16].

4.2. Brief description of previous experimental investigations used for models' validation

The experimental investigations performed by Firmo *et al.* [11, 13] comprised double-lap shear tests on concrete blocks strengthened with CFRP strips, applied according to either EBR or NSM techniques, in which the same epoxy adhesive tested in the present study (*cf.* section 3.1) was used as bonding agent. The specimens were first heated up to temperatures of 20 °C, 55 °C e 90 °C and then loaded up to failure (maintaining the specimens at the target temperature).

Fig. 13 illustrates the geometry of the test specimens and the details of the instrumentation. The two concrete blocks were parallelepiped, with dimensions 120 mm × 120 mm × 350 mm, and were internally reinforced with 2ϕ16 steel rebars (U-shaped, class A500NR) that were also used to apply the mechanical load. The CFRP laminates were 1.4 mm thick, 20 mm wide for the EBR and 10 mm wide for the NSM, and were bonded to the concrete by an epoxy adhesive. In the EBR specimens the adhesive layer was 2 mm thick, whereas in the NSM specimens, the CFRP strips were inserted into slits saw cut in the concrete cover with 15 mm of depth and 5 mm of width, as depicted in **Fig. 13** a).

The instrumentation used in the tests allowed monitoring the following parameters: (i) the load and cross-head displacement of the test machine; (ii) the slip along the bonded length of the CFRP strips (with two high-temperature LVDTs, positioned at the beginning and end of the bonded length, $x = 0$ e $x = 250$ mm, respectively; *cf.* **Fig. 13**c)); and (iii) axial strains along the bonded length of the CFRP strips.

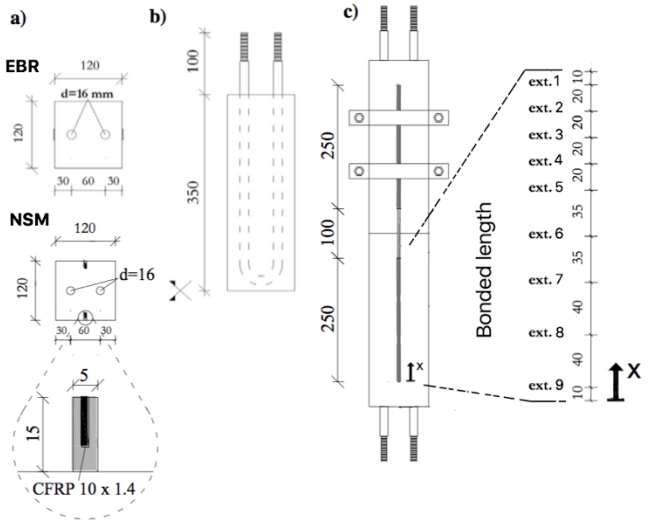

Fig. 13 –Test specimens geometry (a, b) and detail of instrumentation (c) [11, 13].

4.3. Description of the numerical models

4.3.1. Geometry and type elements

The geometry of the FE models developed in the present study replicated that of the test specimens presented above. In order to reduce the computational costs, symmetry simplifications of the model were adopted and only 1/8 of the test specimen volume was modelled. **Fig. 14** and **Fig. 15** illustrate the FE meshes of the EBR and NSM specimens, respectively, for both the a) interface and b) adhesive models. When generating the mesh for concrete, CFRP, adhesive and steel parts, 8-node hexahedral elements (C3D8R) were used.

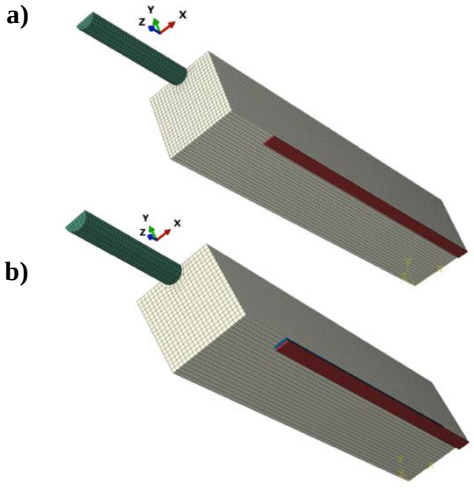

Fig. 14 – EBR specimens mesh: a) interface model; b) adhesive model.

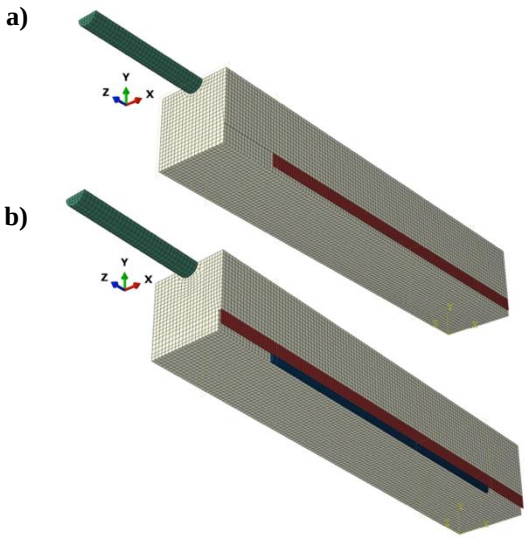

Fig. 15 – NSM specimens mesh: a) interface model; b) adhesive model.

4.3.2. Material properties

All the constituent materials were modelled as linear (without any failure criterion); the defining parameters are listed in **Tab. 3**; it is important to point out that: (i) regarding steel, the maximum stress the reinforcement was subjected to was less than half of its yield stress; (ii) regarding concrete, Arruda *et al.* [16] demonstrated that assuming a linear elastic model for concrete does not lead to significant losses of precision when simulating the CFRP-concrete interaction using global bond *vs.* slip relations and considerably reduces the computational cost; and (iii) although the CFRP strips are orthotropic (comprising mainly a unidirectional reinforcement), in the present application they behave essentially in the longitudinal direction, hence, as a simplification, the CFRP was modelled as a linear elastic isotropic material.

Tab. 3 – Material properties at the considered temperatures.

Material	T [ºC]	E [GPa]	G [GPa]	ν [-]
Concrete – C25/30	20; 55	28.70	-	0.2
	90	22.96		
Steel – A500NR	20; 55; 90	200.00	-	0.3
CFRP – *S&P Laminates CFK 150/2000*	20; 55	152.50	-	0.3
	90	147.00	-	
Adhesive – *S&P Resin 220 Epoxy Adhesive*	20	8.21	4.61	0.3
	55	0.16	0.047	
	90	0.087	0.038	

4.3.3. Loading, boundary conditions and type of analysis

As referred in section 4.3.1, given the triple symmetry of the test specimens, only 1/8 of their volume was modelled. Hence, to insure the proper boundary conditions the following displacements/rotations were restricted: (i) vertical displacements (*y-axis*) at the loaded end of the CFRP strip (*cf.* **Fig. 14**); (ii) vertical displacements and rotations in the plane of symmetry *xz*; and (iii) transverse displacements and rotations in the plane of symmetry *yz*. In addition (i) a perfect bond between the steel rebars and the concrete was assumed; and (ii) the extremity nodes of the steel rebars were fixed in all directions in order to simulate the clamps of the testing machine.

Regarding the adhesive model, a linear elastic analysis was performed, whereas for the interface model a non-linear analysis was adopted. On the latter model the concrete-CFRP bond, simulated by interface contact (in which cohesive bilinear constitutive relationships, represented in **Fig. 16**, were implemented), included a damage initiation criterion after the maximum shear stress value is attained; such criterion corresponds to the descending branch of the bilinear relations shown in **Fig. 16**; these bond *vs.* slip relations were defined by the following three parameters (*cf.* **Tab. 4**): (i) stiffness, K; (ii) maximum shear strength, τ_{LM}; and (iii) ultimate slip, s_{L0}. In order to ensure control of the post-peak structural response, a static non-linear analysis was performed imposing applied displacements.

Tab. 4 – Adopted interface parameters for the considered temperatures.

Parameter	NSM			EBR		
	20°C	**55°C**	**90°C**	**20°C**	**55°C**	**90°C**
K **[MPa/mm]**	300	10	3.5	350	10	3
τ_{LM} **[MPa]**	15	8	3	9	4	1.5
s_{L0} **[mm]**	0.5	0.9	0.95	0.2	0.45	0.6

4.4. Results and discussion

4.4.1. Total load vs. *slip curves*

Fig. 17 depicts the numerical results of the interface and adhesive models together with the experimental results in terms of applied force *vs.* slip at the end of the bonding length ($x = 250$ mm, *cf.* **Fig. 13** c)) for both strengthening techniques and for all temperatures analysed.

Regarding the interface model at ambient temperature, for both EBR and NSM techniques, the numerical models were able to accurately reproduce the non-linear behaviour of the curves, including the high stiffness reduction observed in the brink of collapse. Despite the simplified constitutive model used to simulate the concrete material (modelled as linear elastic) the numerical results adequately reproduce the non-linearity of the mechanical response of the bonded joint. With increasing temperatures, besides the continuous stiffness reduction obtained, the numerical curves presented a behaviour closer to linear, similar to that exhibited by the corresponding experimental curves.

Regarding the adhesive model, at ambient temperature, the initial stiffness of the numerical curves is similar to the experimental ones for both strengthening systems. This result shows that, at ambient temperature and for relatively low loads, the adhesive distortion assumes a more significant relevance for the concrete-CFRP slip value than the sliding at the concrete-adhesive and adhesive-CFRP interfaces (which were not simulated in this model). Thus, it can be concluded that, under these conditions (ambient temperature and relatively low loads), the slip at both interfaces may be considered negligible. As temperature increases, the stiffness of the curves obtained from the adhesive model become

higher than the experimental ones (except for the EBR system at 55 ºC), confirming the relevance of the slip at both interfaces and its importance to the overall structural response. Nevertheless, at 55 °C the stiffness predicted by the adhesive model for the EBR system is very similar to the experimental one. This result, which was not obtained for the NSM system at the same temperature, may be related to the fact that the interface area is lower in the EBR system (and consequently the overall slip is less dependent on slip of the interfaces).

Tab. 5 presents the ratio between the stiffness values predicted by the adhesive model and the experimental data (numerical/experimental) of the NSM and EBR systems. It can be seen that at 20 °C the ratio of both systems is close to unity, thus confirming that the slip at both interfaces may be considered negligible; however, at 90 °C the ratio is between 3.1 and 5.2 times higher, which confirms the increasing relevance of slip at the bonded interfaces at elevated temperature for both strengthening techniques.

Tab. 5 – Ratio between the adhesive model and the experimental stiffness.

	20 °C	**55 °C**	**90 °C**
EBR	1.0	0.7	3.1
NSM	1.3	2.6	5.2

4.4.2. Strain distributions in the CFRP strips

Fig. 18 to **Fig. 21** present the axial strain distributions along the CFRP bonded length obtained from the interface and adhesive models, for different fractions of the failure load and for temperatures up to 90 ºC; in these figures, the experimental results are plotted as dotted lines and the corresponding numerical curves as continuous lines.

Regarding the interface model, the figures show that there is a good agreement between experimental and numerical results. The global bond *vs.* slip relations allowed to simulate the non-linear response of the corresponding curves at ambient temperature, with null deformations at the beginning of the CFRP strip and a peak at the opposite extremity ($x = 0$ and $x = 250$ mm, respectively; *cf.* **Fig. 13** c)). For elevated temperatures, it can be seen that the axial strain distributions along the bonded length become closer to linear (*i.e.*, there is no longer a peak at the top extremity of the CFRP strip) and a reduction of the overall magnitude of the strain distributions as temperature increases. These results are mainly explained by the stiffness reduction of the adhesive and the consequent smoothing of the shear stress and strain distributions along the bonded joint.

Regarding the adhesive model, although there is a reasonable agreement between experimental and numerical results in term of the maximum strain at the end of CFRP strip ($x = 250$ mm, *cf.* **Fig. 13** c)), the linearization of the strain distributions along the bonded length with increasing temperatures is not so pronounced as in the experimental curves. In fact, as expected, since the adhesive model exhibits a stiffer behaviour, the strain distributions show a more pronounced increase near the end of the bonded length. Yet, the reduction of the peak value with the temperature increase can still be seen. It should also be noted that, overall, the values of the strains along the bonded length provided by the adhesive model are slightly lower than the experimental ones, with those differences being higher for the NSM technique.

5. Conclusions

From the results obtained in the experimental study, the following main conclusions can be drawn:

1. As expected, the mechanical properties of the epoxy adhesive presented considerable reductions with increasing temperature, specially within the range that includes the glass transition process (between 35 ºC and 50 ºC);
2. The mechanical response of the adhesive (in both tension and shear) was significantly affected by temperature: whereas a brittle behaviour (linear up to failure) was obtained at ambient temperature and a markedly non-linear response was observed at higher temperatures, especially at 50 °C and 70 °C;
3. The ultimate deformation capacity under tensile and shear stresses exhibited a non-monotonic variation with temperature (*i.e.*, it increased from 35 °C to 50 °C, and it decreased for higher temperatures), unlike the tensile and shear strengths, which decreased monotonically with increasing temperature;
4. For temperatures higher than the T_g, the degradation of the stiffness properties is significantly more pronounced than that exhibited by the corresponding strengths – becoming almost negligible beyond 50 °C;
5. The model proposed by Gibson *et al.* [19] was able to accurately simulate the reduction with temperature of the mechanical properties determined in the experimental campaign.

Regarding the results obtained in the numerical study, the following main conclusions can be drawn:

1. As expected, the results obtained from the interface model, presented a very good agreement with experimental data in terms of total load *vs.* slip response and strain distributions in the CFRP strip along the bonded length;
2. At ambient temperatures, the results obtained from the adhesive model predicted accurately the total load *vs.* slip response for relatively low loads, which indicated that the slip at both interfaces may be considered negligible; on the other hand, at higher temperatures, the difference between the experimental and numerical results pointed out and allowed quantifying the relevance of the occurrence of slip at the concrete-adhesive and adhesive-CFRP interfaces.
3. Regarding the strains in the CFRP along the bonded length, both numerical models were able to accurately simulate the non-linear response observed at ambient temperature, as well as the strain linearization along the bonded length with increasing temperatures.

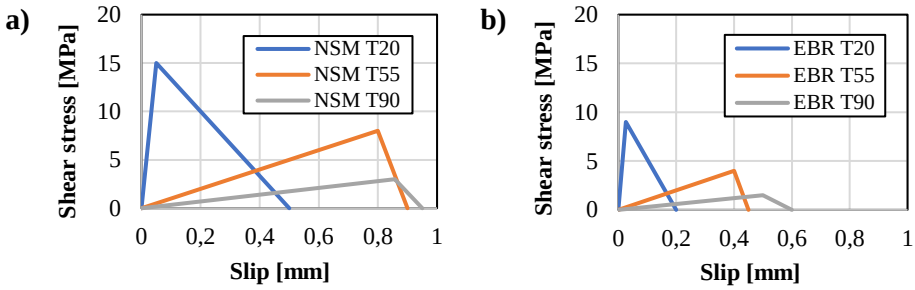

Fig. 16 – Bond *vs.* slip laws for a) NSM and b) EBR specimens for the considered temperatures.

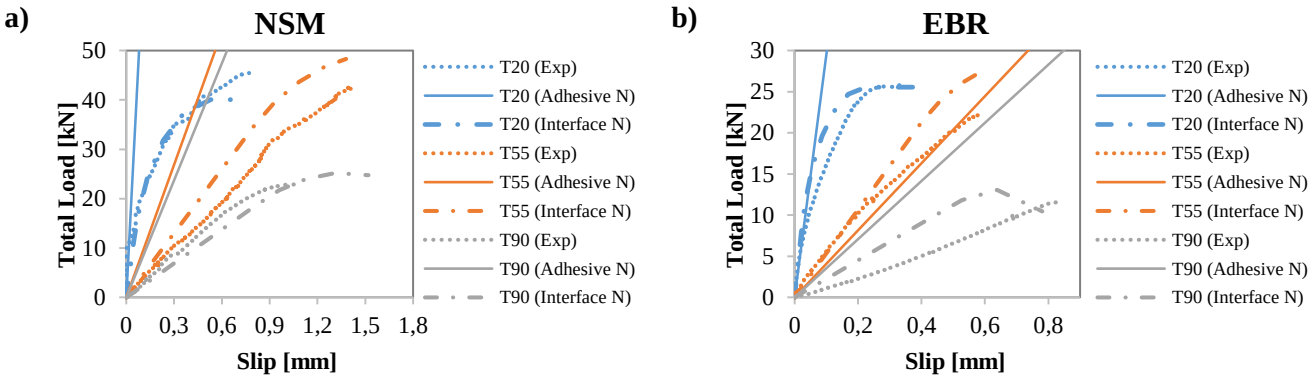

Fig. 17 – Numerical (N; according to the interface and adhesive model) and experimental (Exp) total load *vs.* slip curves for the considered temperatures: a) NSM; and b) EBR specimens.

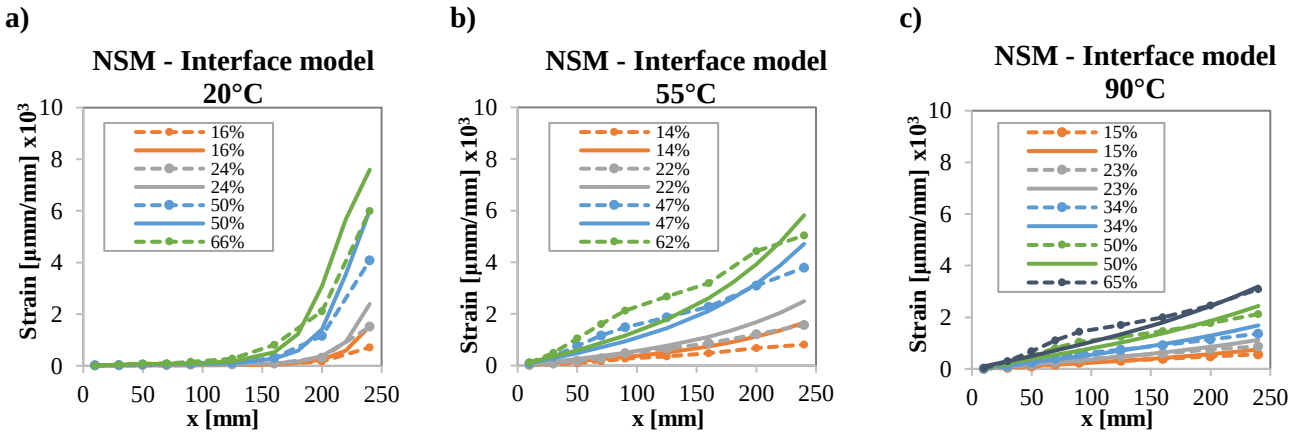

Fig. 18 - Experimental (dashed) and numerical (continuous) according to interface model longitudinal axial strains in the NSM series for several fractions of the failure load and different temperatures: a) 20 ºC; b) 55 ºC; and c) 90 ºC.

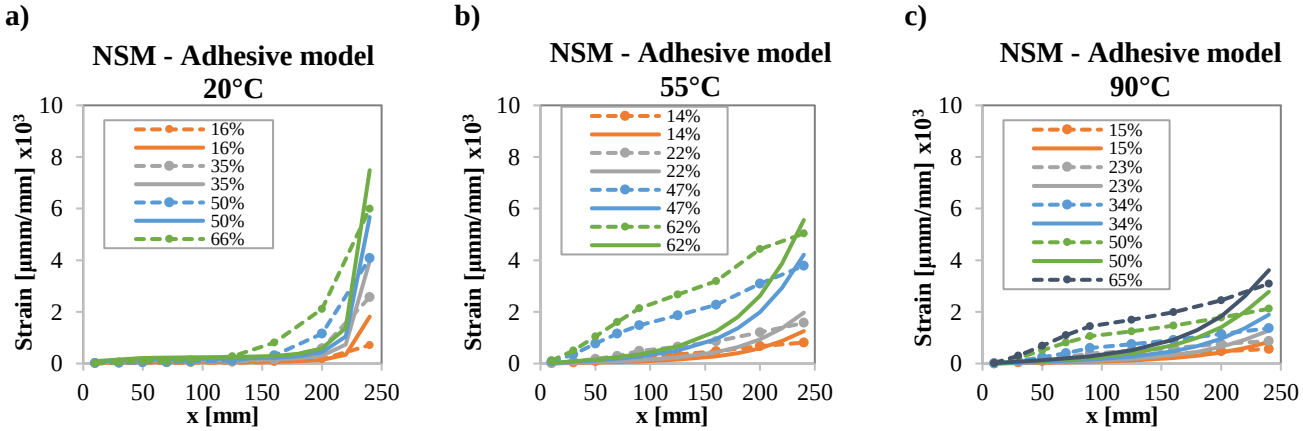

Fig. 19 - Experimental (dashed) and numerical (continuous) according to adhesive model longitudinal axial strains in the NSM series for several fractions of the failure load and different temperatures: a) 20 ºC; b) 55 ºC; and c) 90 ºC.

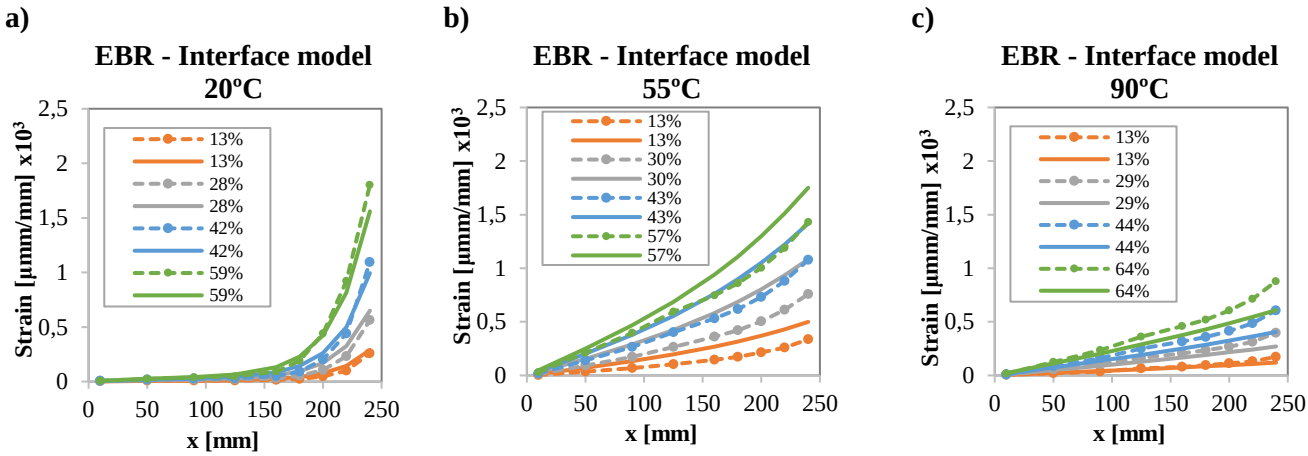

Fig. 20 - Experimental (dashed) and numerical (continuous) according to interface model longitudinal axial strains in the EBR series for several fractions of the failure load and different temperatures: a) 20 ºC; b) 55 ºC; and c) 90 ºC.

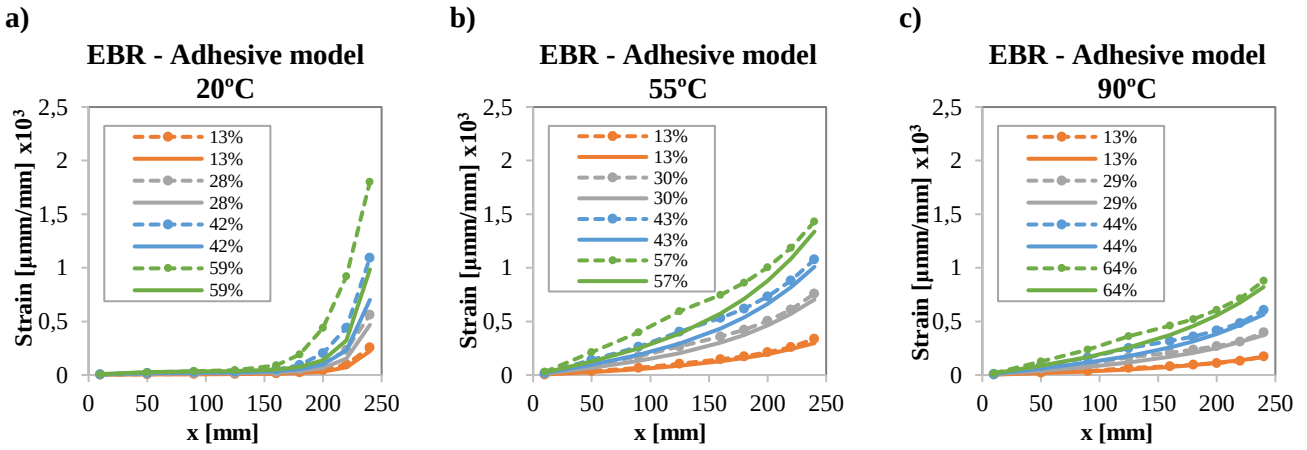

Fig. 21 - Experimental (dashed) and numerical (continuous) according to adhesive model longitudinal axial strains in the EBR series for several fractions of the failure load and different temperatures: a) 20 ºC; b) 55 ºC; and c) 90 ºC.

6. References

[1] Bakis, C. E., Bank, L. C., Brown, V. L., Cosenza, E., Davalos, J. F., Lesko, J. J., Machida, A., Rizkalla, S. H. and Triantafillou, T. C., *Fiber-reinforced polymer composites for construction — state-of-the-art review*, Journal Of Composites For Construction, Vol. 6, No. 2, pp. 73–87, 2002.

[2] Firmo, J. P., Correia, J. R. and Bisby, L. A., *Fire behaviour of FRP-strengthened reinforced concrete structural elements: A state-of-the-art review*, Composites Part B, Vol. 80, pp. 198–216, 2015.

[3] Bascom, W. D. and Cottington, R. L., *Effect of Temperature on the Adhesive Fracture Behavior of an Elastomer-Epoxy Resin*, The Journal of Adhesion, Vol. 7, No. 4, pp. 333–346, 1976.

[4] Moussa, O., Vassilopoulos, A. P., De Castro, J. and Keller, T., *Time-temperature dependence of thermomechanical recovery of cold-curing structural adhesives*, International Journal of Adhesion and Adhesives, Vol. 35, pp. 94–101, Elsevier, 2012.

[5] Blontrock, H., *Analysis and modeling of the fire resistance of concrete elements with externally bonded FRP reinforcement*, PhD thesis in Civil Engineering, Ghent University, Ghent, Belgium, 2003.

[6] Klamer, E. L., Hordijk, D. A. and Janssen, H. J. M., *The influence of temperature on the debonding of externally bonded CFRP*, Proceedings 7th Int. Symposium on Fiber Reinforcement Polymer Reinforcement for Concrete Structures (FRPRCS-7), pp. 1551–1570, 2005.

[7] Klamer, E. L., *Influence of temperature on concrete beams strengthened in flexure with CFRP*, PhD thesis in Civil Engineering, Eindhoven University of Technology, Eindhoven, Netherlands, 2009.

[8] Burke, P. J., Bisby, L. A. and Green, M. F., *Effects of elevated temperature on near surface mounted and externally bonded FRP strengthening systems for concrete*, Cement and Concrete Composites, Vol. 35, No. 1, pp. 190–199, Jan. 2013.

[9] Wu, Z., Iwashita, K., Yagashiro, S., Ishikawa, T. and Hamaguchi, Y., *Temperature effect on bonding and debonding behavior between FRP sheets and concrete*, Journal of the Society of Materials Science, Japan, Vol. 54, No. 5, pp. 474–480, 2005.

[10] Gamage, J. C. P. H., Wong, M. B. and Al-Mahadi, R., *Performance of CFRP strengthened concrete members under elevated temperatures*, Proceeding of the International Sysposium on Bond Behaviour of FRP in Structures (BBFS 2005), pp. 113–118, 2005.

[11] Firmo, J. P., Correia, J. R., Pitta, D., Tiago, C. and Arruda, M. R. T., *Experimental characterization of the bond between externally bonded reinforcement (EBR) CFRP strips and concrete at elevated temperatures*, Cement and Concrete Composites, Vol. 60, pp. 44–54, 2015.

[12] Yu, B. and Kodur, V. K. R., *Effect of high temperature on bond strength of near-surface mounted FRP reinforcement*, Composite Structures, Vol. 110, No. 1, pp. 88–97, 2014.

[13] Firmo, J. P., Pitta, D., Correia, J. R., Tiago, C. and Arruda, M. R. T., *Bond behavior at high temperatures between near surface mounted (NSM) CFRP strips and concrete*, Journal of Composites for Construction, 2014.

[14] Gao, W. Y., Teng, J. G., Dai, J., *Effect of temperature variation on the full-range behavior of FRP-to-concrete bonded joints*, Journal of Composites for Construction, Vol. 16, No. 6, pp. 671-683, 2012.

[15] Dai, J., Gao, W. Y., Teng, J. G. and Asce, M., *Bond-slip model for FRP laminates externally bonded to concrete at elevated temperature*, Journal of Composites for Construction, Vol. 17, No. 2, pp. 217-228, 2013.

[16] Arruda, M. R. T., Firmo, J. P., Correia, J. R. and Tiago, C., *Numerical modelling of the bond between concrete and CFRP laminates at elevated temperatures*, Engineering Structures, Vol. 110, pp. 233–243, 2016.

[17] ASTM D 5379, *Standard Test Method for Shear Properties of Composite Materials by the V-Notched*, 2005.

[18] ISO 527-1, *Plastics — Determination of tensile properties - Part 1: General principles*, 1996.

[19] Gibson, A. G., Wu, Y.-S., Evans, J. T. and Mouritz, A. P., *Laminate theory analysis of composites under load in fire*, Journal of Composite Materials, Vol. 40, No. 7, pp. 639–658, 2006.

[20] Firmo, J. P., *Fire behaviour of reinforced concrete structures strengthened with CFRP strips*, PhD thesis in Civil Engineering, Instituto Superior Técnico, Lisboa, 2015.

[21] SIMULIA; ABAQUS 6.11, *Analysis User's Manual*, 2011.